CHEMISTRY OF MATERIALS

Article

Multi-Dipolar Chromophores Featuring Phosphine Oxide as Joint Acceptor: A New Strategy towards High-Efficiency Blue Thermally Activated Delayed Fluorescence Dyes

Chunbo Duan, Jing Li, Chunmiao Han, Dongxue Ding, He Yang, Ying Wei, and Hui Xu

Chem. Mater., **Just Accepted Manuscript** • DOI: 10.1021/acs.chemmater.6b01691 • Publication Date (Web): 21 Jul 2016

ACS Publications

Chemistry of Materials is published by the American Chemical Society. 1155 Sixteenth Street N.W., Washington, DC 20036

Multi-Dipolar Chromophores Featuring Phosphine Oxide as Joint Acceptor: A New Strategy towards High-Efficiency Blue Thermally Activated Delayed Fluorescence Dyes

Chunbo Duan,[‡] Jing Li,[‡] Chunmiao Han, Dongxue Ding, He Yang, Ying Wei *and Hui Xu*[*]

Key Laboratory of Functional Inorganic Material Chemistry, Ministry of Education, Heilongjiang University, 74 Xuefu Road, Harbin 150080, P. R. China

ABSTRACT: Blue thermally activated delayed fluorescence (TADF) dyes are basically the combinations of strong acceptors and weak donors. Contrarily, in this work, a weak acceptor P=O group was employed to construct a series of weak acceptor-strong donor (WASD)-type emitters with phenoxazine donor, namely 10-(4-(diphenylphosphoryl)phenyl)-10H-phenoxazine (**SPXZPO**), 10,10'-(4,4'-(phenylphosphoryl)bis(4,1-phenylene))bis(10H-phenoxazine) (**DPXZPO**) and 10,10',10"-(4,4',4"-phosphoryltris(benzene-4,1-diyl))tris(10H-phenoxazine) (**TPXZPO**). Owing to the insulating effect of P=O on conjugation extension and intramolecular electronic communications, the photoluminescence spectra of these molecules are almost unchanged, manifesting the superiority of WASD structure in emission color preservation. Simultaneously, the multi-dipolar characteristics of **TPXZPO** enhances the intramolecular

charge transfer (ICT), facilitating the reverse intersystem crossing (RISC) for higher TADF efficiency and shorter lifetime. In consequence, **TPXZPO** realized the desired pure-blue electroluminescence peaked at 464 nm, accompanied by the favorable external quantum efficiency (EQE, η_{ext}) up to 15.3%, the 100% exciton utilization ratio and reduced efficiency roll-offs. Its complementary full-TADF white organic light-emitting diodes (OLED) also achieved the maximum η_{ext} as high as 16.3%, among the best results of white TADF devices reported so far. As the first example of P=O-based WASD-type blue TADF dyes, the success of **TPXZPO** is the result of the comprehensive and harmonized effects of P=O joint on controlling conjugation and intramolecular electronic communication and multi-dipolar structure on ICT enhancement.

1. Introduction

In recent years, thermally activated delayed fluorescence (TADF) materials and diodes attract extensive attention, owing to their predominant superiorities in energy conservation, environmental protection and low cost.[1-4] As heavy-metal-free pure organic chromophores with bipolar structures, TADF emitters can achieve near-zero singlet-triplet splitting (ΔE_{ST}) for efficient reverse intersystem crossing (RISC) from triplet (T_1) to singlet (S_1) excited states.[5-8] Consequently, all electrogenerated excitons can be converged to the radative S_1 states for 100% theoretically internal quantum efficiency (IQE, η_{int}).[9-11] It is known that RISC rate constant (k_{RISC}) follows Boltzmann distribution relation as $k_{RISC} \propto \exp(-\Delta E_{ST}/k_B T)$. In this case, ΔE_{ST} should be as small as possible to facilitate TADF, which is twice of the electron exchange energy (J) expressed as:

$$\Delta E_{ST} = 2J = 2\iint \Psi_L(1)\Psi_H(2)\left(\frac{e^2}{r_1 - r_2}\right)\Psi_L(2)\Psi_H(1)dr_1 dr_2 \quad (1)$$

$$\Delta E_{ST} = 2(\Psi_{\mathrm{H}}\Psi_L|r_{12}^{-1}|\Psi_{\mathrm{H}}\Psi_L) + 2(\Psi_{\mathrm{H}}\Psi_L|\hat{f}_{XC}^{\alpha\beta}|\Psi_{\mathrm{H}}\Psi_L) \quad (2)$$

where ψ_H and ψ_L refer to the wave functions of the highest occupied and lowest unoccupied molecular orbitals (HOMO and LUMO), respectively, and $\hat{f}_{XC}^{\alpha\beta}$ represents the density functional theory (DFT) exchange-correlation (XC) kernel with spin labels α or β. Therefore, ΔE_{ST} is in direct proportion to the overlap integral of $<\psi_H|\psi_L>$. Consequently, most of TADF dyes are donor-acceptor (D-A) systems with bipolar characteristics, in virtue of strong electron donating and withdrawing effects on the HOMO-LUMO separation. In this sense, the construction of efficient TADF emitters is actually embodied in selecting and optimizing the combination of donors and acceptors.[12-14]

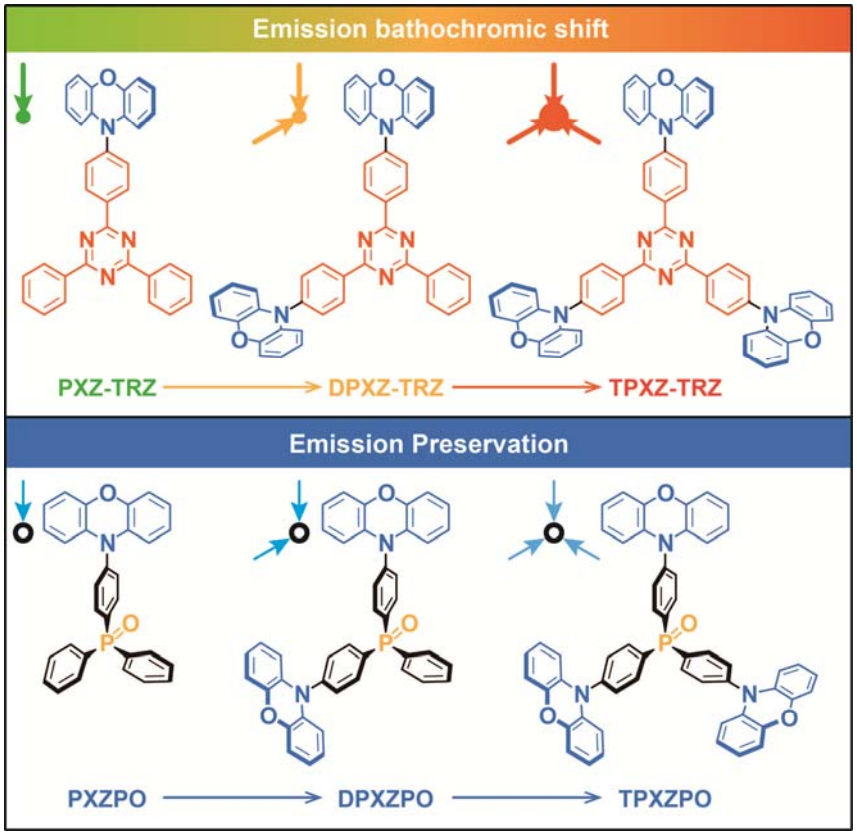

Figure 1. The opposite influences of donor density on emission colors for ***x*PXZ-TRZ** and ***x*PXZPO**.

In comparison to various arylamine-type donors, the acceptors for TADF dyes reported are mainly limited in benzonitrile, *N*-heterocycles, carbonyl and sulfone, restraining the diversity of material structures on some level.[3] Therefore, the acceptor development becomes imperative, and some highly efficient TADF emitters with novel acceptor units spring up, such as thioxanthone[15] and thianthrene-9,9',10,10'-tetraoxide[16] for green and yellow dyes. In general, the acceptor units employed so far can be divided into two types, viz. conjugated (benzonitrile, pyridine, triazine, thioxanthone etc.) and insulating acceptors (carbonyl and sulfone, etc.). It is noteworthy that when employing conjugated acceptors, the overlapped electron-donating and withdrawing effects and intramolecular conjugation extension in multiple D-A systems invariably render the bathochromic shift of their photoluminescence (PL) and electroluminescence (EL). For instance, Adachi group reported a series of phenoxazine-triazine hybrids with green, yellow and orange emissions, along with the increase of their phenoxazine group numbers from 1 to 3 (**Figure 1**).[6] In this case, the weak donor groups, e.g. carbazole dendrons, should be adopted for blue emission and concentrated on one side of the molecules to form mono-bipolar configurations.[17-19] On contrary, insulating acceptors, e.g. carbonyl[20] and sulfone[21] groups, can effectively interrupt intramolecular conjugation and electronic communications, therefore predominant in the construction of blue TADF dyes with multi-dipolar characteristics. Nevertheless, the strong electron-withdrawing effects of carbonyl and sulfone groups render the deep LUMOs around -3.0 eV, while, photon energy of blue light corresponds to the HOMO-LUMO energy gaps of ~2.8 eV and thereby the deep HOMOs around -5.8 eV. Consequently, still only weak donor groups, such as carbazole and acridine, etc., can be incorporated to achieve desired blue

emissions with Commission Internationale Ed I'eclairage (CIE) coordinates of x+y < 0.4; otherwise, the employment of strong donor groups, e.g. phenoxazine, would render the significant emissive bathochromic shift beyond 40 nm,[22-23] which remarkably restrains the development of blue TADF emitters and should be one of the main reasons making blue devices as the bottleneck of TADF technology.

It is noteworthy that all of the reported blue TADF dyes are strong acceptor-weak donor (SAWD) systems, whose donor and acceptor units give rise to the HOMO and LUMO deeper than -5.9 and -2.9 eV.[3] Therefore, as a reversal, it is rational to establish the opposite design strategy of constructing weak acceptor-strong donor (WASD) combinations with the HOMO and LUMO shallower than -5.7 and -2.7 eV, respectively, as promising alternatives, through controlling HOMO-LUMO energy gaps around ~2.8 eV for blue emission and effective intramolecular charge transfer (ICT) for small ΔE_{ST}. In this contribution, as a proof of concept, phosphine oxide (P=O) group with appropriate electron withdrawing effect is incorporated as joint acceptor to construct a series of WASD-type blue TADF chromophores with one, two and three phenoxazine donors, respectively, namely 10-(4-(diphenylphosphoryl)phenyl)-10H-phenoxazine (**SPXZPO**), 10,10'-(4,4'-(phenylphosphoryl)bis(4,1-phenylene))bis(10H-phenoxazine) (**DPXZPO**) and 10,10',10''-(4,4',4''-phosphoryltris(benzene-4,1-diyl))tris(10H-phenoxazine) (**TPXZPO**) with collective name of ***x*PXZPO** (**Figure 1**). As an insulating linkage, P=O groups effectively suppress the conjugation extensions and intramolecular electronic communications. Consequently, **TPXZPO** with tri-dipolar characteristics realizes the blue emission with negligible bathochromic shift less than 10 nm, compared to bi-dipolar **DPXZPO** and mono-dipolar **SPXZPO**. Simultaneously, the multi-dipolar structure of **TPXZPO** effectively amplifies its ICT effect and increases molecular orbital density, giving rise to the remarkably

reduced ΔE_{ST} of 0.11 eV and potential multi-channel and accelerated RISC process, which further endow **TPXZPO** with the shortest delayed fluorescence (DF) lifetime and the highest photoluminescence quantum yields (PLQY) of prompt fluorescence (PF) and DF among ***x*PXZPO**. As the result, on the basis of a conventional device configuration, **TPXZPO** successfully realized the desired true-blue EL emission peaked at 464 nm with favorable CIE coordinates of (0.17, 0.20) and the impressive external quantum efficiency (EQE, η_{ext}) beyond 15%. With incorporation of a yellow dopant 3,4,5,6-tetrakis(3,6-diphenylcarbazol-9-yl)-1,2-dicyanobenzene (4CzPNPh), **TPXZPO** further supported its full-TADF complementary white devices with a high η_{ext} up to 16.3%. This work convincingly verifies the effectiveness of WASD strategy in developing high-performance blue TADF dyes and would doubtlessly promote the practical application of TADF technology in display and lighting.

2. Experimental Section

Materials and Instruments: All the reagents and solvents used for the synthesis of the compounds were purchased from Aldrich and Acros companies and used without further purification.

^{1}H NMR spectra were recorded using a Varian Mercury plus 400NB spectrometer relative to tetramethylsilane (TMS) as internal standard. Molecular masses were determined by a FINNIGAN LCQ Electro-Spraying Ionization-Mass Spectrometry (ESI-MS), or a MALDI-TOF-MS. Elemental analyses were performed on a Vario EL III elemental analyzer. Absorption and photoluminescence (PL) emission spectra of the target compound were measured using a SHIMADZU UV-3150 spectrophotometer and a SHIMADZU RF-5301PC spectrophotometer, respectively. Thermogravimetric analysis (TGA) and differential scanning calorimetry (DSC) were performed on Shimadzu DSC-60A and DTG-60A thermal analyzers under nitrogen

atmosphere at a heating rate of 10 °C min-1. The morphological characteristics of the films were measured with an atom force microscope (AFM) Agilent 5100 under the tapping mode. Cyclic voltammetric (CV) studies were conducted using an Eco Chemie B. V. AUTOLAB potentiostat in a typical three-electrode cell with a glassy carbon working electrode, a platinum wire counter electrode, and a silver/silver chloride (Ag/AgCl) reference electrode. All electrochemical experiments were carried out under a nitrogen atmosphere at room temperature in dichloromethane. Phosphorescence spectra were measured in dichloromethane using an Edinburgh FPLS 920 fluorescence spectrophotometer at 77 K cooling by liquid nitrogen with a delay of 300 μs using Time-Correlated Single Photon Counting (TCSPC) method with a microsecond pulsed Xenon light source for 2 μs-10 s lifetime measurement, the synchronization photomultiplier for signal collection and the Multi-Channel Scaling Mode of the PCS900 fast counter PC plug-in card for data processing. The temperature-variable transient emission decay spectra were measured with a temperature controller over a range of 77-310 K. The ***x*PXZPO** doped DPEPO films (100 nm) were prepared through vacuum evaporation for optical analysis and AFM measurement. Photoluminescence quantum yields (PLQY) of these films were measured through a labsphere 1-M-2 (ϕ = 6") integrating sphere coated by Benflect with efficient light reflection in a wide range of 200-1600 nm, which was integrated with FPLS 920. The absolute PLQY determination of the sample was performed by two spectral (emission) scans, with the emission monochromator scanning over the Rayleigh scattered light from the sample and from a blank substrate. The first spectrum recorded the scattered light and the emission of the sample, and the second spectrum contained the scattered light of Benflect coating. The integration and subtraction of the scattered light parts in these two spectra arrived at the photon number absorbed by the samples (N_a); while, integration of the emission of the samples to

calculate the emissive photon number (N_e). Then, the absolute PLQY (η) can be estimated according to the equation of $\eta = N_e/N_a$. Spectral correction (emission arm) was applied to the raw data after background subtraction, and from these spectrally corrected curves the quantum yield was calculated using aF900 software wizard.

Synthesis of 10-(4-bromophenyl)-10H-phenoxazine (**PXZPhBr**): in Ar, **PXZ** (1.84 g, 10 mmol), 1-bromo-4-iodobenzene (6.23 g, 22 mmol), CuI (0.19 g, 8 mmol) and anhydrous K_2CO_3 (2.76 g, 20 mmol) were mixed and heated to 180 ^oC for 24 h under stirring. The reaction was cooled to room temperature and quenched by addition of water (50 mL). The mixture was exacted with CH_2Cl_2 (3×30 mL). The organic phase was combined and dried with anhydrous Na2SO4. The solvent was removed under vacuum. The residue was purified with flash column chromatography to afford white powder of 1.46 g with a yield of 45%. ^1H NMR (TMS, $CDCl_3$, 400 MHz): δ = 7.977(d, J = 7.6 Hz, 1H), 7.777 (d, J = 7.6 Hz, 1H), 7.307 (d, J = 7.6 Hz, 1H), 7.155 (d, J = 7.6 Hz, 1H), 6.754- 6.534 (m, 6H), 5.967 ppm (d, J = 7.6 Hz, 1H); LDI-TOF: m/z (%): 337 (100) [M^+]; elemental analysis (%) for $C_{18}H_{12}BrNO$: C 63.92, H 3.58, N 4.14; found: C 63.95, H 3.61, N 4.17.

General synthetic procedure of phosphorylation reaction: in Ar, **PXZPhBr** (3 mmol) was dissolved in anhydrous THF (30 mL). The solution was cooled to-78 ^oC, then *n*-BuLi (2.5 M in hexane, 1.5 mL, 3.6 mmol) was added in dropwise. The mixture was stirred for 2 h, and then added with diphenylchlorophosphine (for **SPXZPO**, 3.6 mmol), phenyldichlorophosphine (for **DPXZPO**, 1.5 mmol) or phosphorus trichloride (for **TPXZPO**, 1 mmol). After addition, the mixture was gradually warmed to room temperature and stirred for 2 h. Then, the reaction was quenched by water addition. The mixture was extracted with CH_2Cl_2 (3×30 mL). The CH_2Cl_2 solution was added with 30% H_2O_2 (3.1 mL, 24 mmol) at 0 ^oC and stirred for 4 h. The mixture

was extracted with CH_2Cl_2 (3×30 mL) again. The organic phase was combined and dried with anhydrous Na_2SO_4. Then, the solvent was removed in *vacuo*. The crude product was purified with flash column chromatography.

SCHEME 1. Synthetic procedure of ***x*PXZPO**: (i) 1-bromo-4-iodobenzene, CuI, K_2CO_3, 180 ^oC, 24 h; (ii) n-BuLi, THF, -78 ^oC, 2h; phosphine regent, -78 ^oC, 1h; 30%H_2O_2, CH_2Cl_2, 0 ^oC, 4h.

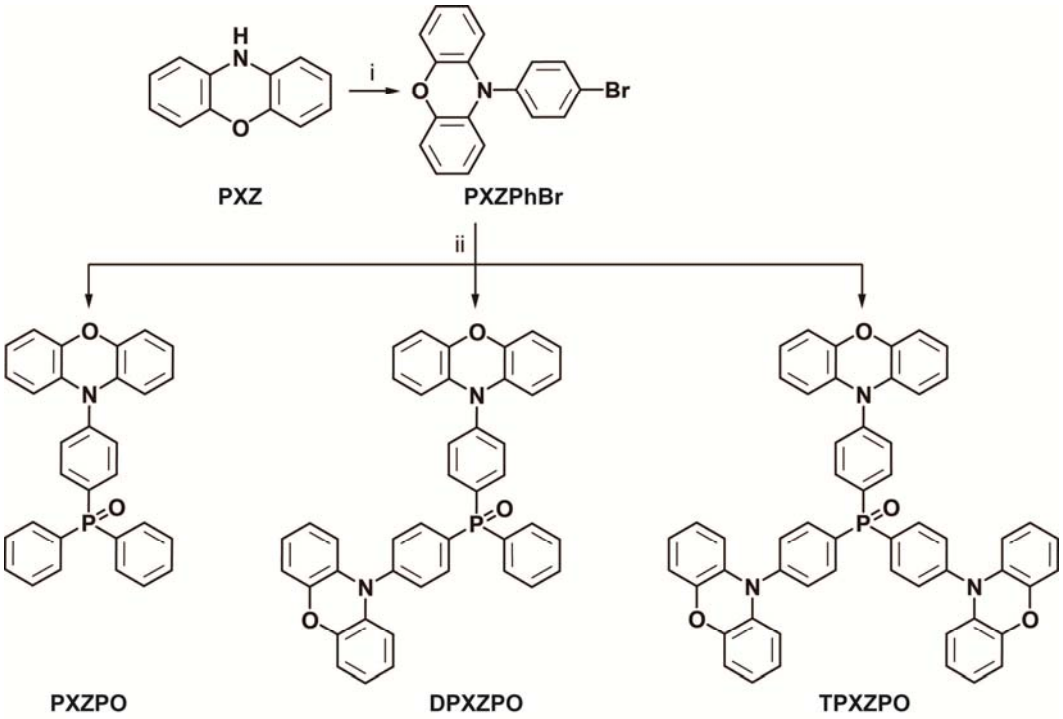

10-(4-(Diphenylphosphoryl)phenyl)-10H-phenoxazine (**SPXZPO**): white powder of 0.91 g with a yield of 57%. ^{1}H NMR (TMS, $CDCl_3$, 400 MHz): δ = 7.907-7.859 (dd, J_1 = 8.0 Hz, J_2 = 8.4 Hz, 2H), 7.771-7.720 (dd, J_1 = 8.4 Hz, J_2 = 12.0 Hz, 4H), 7.616-7.576 (m, 2H),7.544-7.500 (m, 4H), 7.461 (d, J = 6.4Hz, 2H), 6.707-6.705 (m, 6H), 5.938-5.925 ppm (m, 2H); LDI-TOF: m/z (%): 459 (100) [M^+]; elemental analysis (%) for $C_{30}H_{22}NO_2P$: C 78.42, H 4.83, N 3.05; found: C 78.44, H 4.82, N 3.08.

10,10'-(4,4'-(Phenylphosphoryl)bis(4,1-phenylene))bis(10H-phenoxazine) (**DPXZPO**): white powder of 0.91 g with a yield of 57%. ^{1}H NMR (TMS, $CDCl_3$, 400 MHz): δ = 7.982- 7.933 (dd, J_1 = 8.0 Hz, J_2 = 8.4 Hz, 4H), 7.851-7.803 (m, 2H), 7.659-7.638(t, J = 7.2 Hz, 1H), 7.614-7.570 (m, 2H), 7.539 (dd, J_1 = 8.0 Hz, J_2 = 2.0 Hz, 4H), 6.72-6.606 (m, 12H), 5.977 ppm (d, J = 7.6Hz, 4H); LDI-TOF: m/z (%): 640 (100) [M^+]; elemental analysis (%) for $C_{42}H_{29}N_2O_3P$: C 78.74, H 4.56, N 4.37; found: C 78.774, H 4.58, N 4.42.

10,10',10''-(4,4',4''-phosphoryltris(benzene-4,1-diyl))tris(10H-phenoxazine) (**TPXZPO**): white powder of 0.91 g with a yield of 57%. ^{1}H NMR (TMS, $CDCl_3$, 400 MHz): δ = 8.050-8.001 (dd, J_1 = 8.0 Hz, J_2 = 8.0 Hz, 6H), 7.612- 7.591 (td, J_1 = 8.4 Hz, J_2 = 2.0 Hz, 6H), 6.747-6.624 (m, 18H), 6.018 ppm (d, J = 7.6Hz, 6H); LDI-TOF: m/z (%): 821 (100) [M^+]; elemental analysis (%) for $C_{54}H_{36}N_3O_4P$: C 78.92, H 4.42, N 5.11; found: C 78.95, H 4.41, N 5.17.

DFT and TDDFT Calculation: DFT computations were carried out with different parameters for structure optimizations and vibration analyses. The ground state configuration was established according to single crystal data. The singlet and triplet states of ***x*PXZPO** in vacuum were optimized by the restricted and unrestricted formalism of Beck's three-parameter hybrid exchange functional[24] and Lee, and Yang and Parr correlation functional[25] B3LYP/6-31G(d,p), respectively. The fully optimized stationary points were further characterized by harmonic vibrational frequency analysis to ensure that real local minima had been found without imaginary vibrational frequency. The total energies were also corrected by zero-point energy both for the ground state and triplet state. Natural transition orbital (NTO) analysis was performed on the basis of optimized ground-state geometries at the level of B3LYP/6-31G(d,p).[26] The contours were visualized with Gaussview 5.0. All computations were performed using the Gaussian 09 package.[27]

Device Fabrication and Testing: Before loading into a deposition chamber, the ITO substrate was cleaned with detergents and deionized water, dried in an oven at 120 °C for 4 h, and treated with oxygen plasma for 3 min. Devices were fabricated by evaporating organic layers at a rate of 0.1-0.2 nm s^{-1} onto the ITO substrate sequentially at a pressure below 4×10^{-4} Pa. Onto the electron-transporting layer, a layer of LiF with 1 nm thickness was deposited at a rate of 0.1 nm s^{-1} to improve electron injection. Finally, a 100-nm-thick layer of Al was deposited at a rate of 0.6 nm s^{-1} as the cathode. The emission area of the devices was 0.09 cm^2 as determined by the overlap area of the anode and the cathode. After fabrication, the devices were immediately transferred to a glove box for encapsulation with glass cover slips using epoxy glue. The EL spectra and CIE coordinates were measured using a PR655 spectra colorimeter. The current-density-voltage and brightness–voltage curves of the devices were measured using a Keithley 4200 source meter and a calibrated silicon photodiode. All the measurements were carried out at room temperature under ambient conditions. For each structure, four devices were fabricated in parallel to confirm the performance repeatability. To make conclusions reliable, the data reported herein were most close to the average results.

3. Results and Discussions

3.1. Design, Synthesis and Characterization

To achieve efficient blue TADF from WASD systems, an ideal weak acceptor should have: (i) appropriate electron-withdrawing ability; (ii) limited excited energy reduction for blue emission and (iii) tunable strength of electronic coupling with donor to provide effective ICT and facilitate RISC. In response to these concerns, P=O group seems promising as a typical "weak" acceptor with moderate electron-withdrawing effect, which is widely adopted to construct multifunctional fluorophors[28-33] and electron transporting materials (ETM)[34-42]. Especially, in recent years, P=O-

involved high-performance ambipolar host materials with preserved high excited energy for both blue phosphorescence[43-63] and TADF[64-65] devices have emerged, whose successive C-P σ bonds have the insulating effect on conjugation extension and excessive intramolecular interplays. Significantly, when using P=O as a joint, it can bond with three aryl groups at the most to form the single, double and triple-dipolar configurations with successively enhanced ICT. In this sense, the electron-withdrawing and conjugation-insulating effects and multi-functionability are successfully integrated by P=O group, making it almost ideal as acceptor to developing blue-emitting multi-dipolar chromophores.

To manifest the superiority of WASD systems in emission color preservation, phenoxazine was adopted with strong electron-donating ability to form D-A structures with P=O group. Three homologues, namely **SPXZPO**, **DPXZPO** and **TPXZPO**, with one, two and three phenoxazine groups, respectively, were constructed to verify the influence of multiple ICT configuration on ΔE_{ST}. ***x*PXZPO** can be conveniently prepared from 10-(4-bromophenyl)-phenoxazine through a facile two-step reaction of successive lithiation and phosphorylation with a good yield of ~60% (**Scheme 1**). Their chemical structures were fully characterized with nuclear magnetic resonance (NMR) spectroscopy, mass spectroscopy and elemental analysis.

3.2. Thermal and Morphological Properties

The tetrahedral geometry of P=O group is beneficial to form three-dimensional structure and increases the molecular rigidity, therefore enhancing the thermal performance and morphological stability. The thermal gravity (TG) and differential scanning calorimetry (DSC) analysis of ***x*PXZPO** was performed (**Figure S1** and **Table 1**). All of the materials revealed the high thermal stability with the temperature of decomposition (T_d) more than 350 ^{o}C, making preparation of nanometer-scaled thin film through *vacuum* evaporation feasible. In comparison to that of

SPXZPO, T_d of **DPXZPO** dramatically increases by 70 °C; while, **TPXZPO** showed the highest T_d of 459 °C among ***x*PXZPO**. Although no glass transition temperature was observed, the melting point (T_m) of **SPXZPO** is 228 °C, which is comparable to 240 °C of **DPXZPO**. However, T_m of **TPXZPO** is as high as 302 °C with a significant increment of >60 °C. The similar thermal stability of **DPXZPO** and **TPXZPO** is in accord with their comparable molecular rigidity; while, the remarkably increased T_m of **TPXZPO** should be attributed to its highly improved molecular symmetry, rendering the strong intermolecular interactions and morphological stability. Although it seems the thermal and morphological stability of ***x*PXZPO** is in direct proportion to the number of phenoxazine.

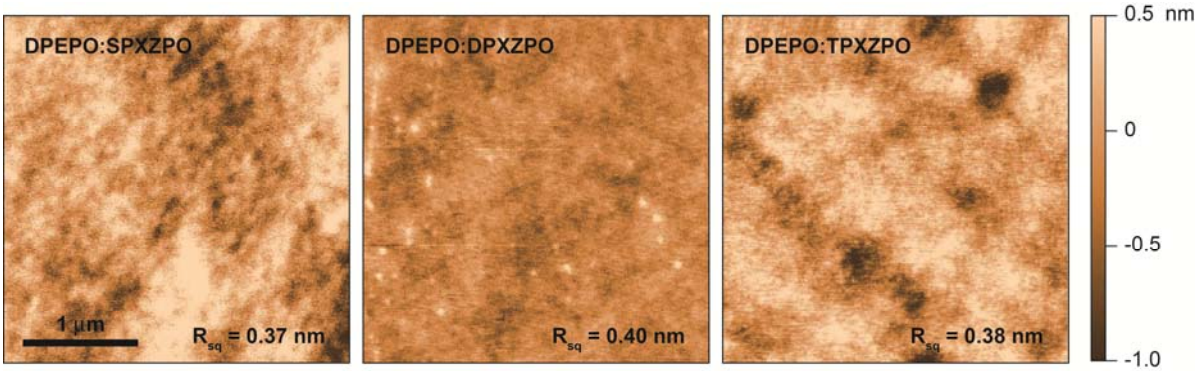

Figure 2. AFM images of *vacuum*-evaporated ***x*PXZPO**-doped **DPEPO** thin films (area: 3×3 μm^2, thickness: 100 nm, doping concentration: 10%wt).

The similarity of ***x*PXZPO** and P=O-based high-energy-gap hosts in molecular constitution and polarity could improve the host-dopant compatibility.[42, 66] ***x*PXZPO** were doped in a typical blue TADF host bis(2-(di(phenyl)phosphino)-phenyl)ether oxide (DPEPO)[67] to form *vacuum*-codeposited films with concentration of 10%wt. and thickness of 100 nm, whose morphologies were investigated with the atom force microscopy (AFM) (**Figure 2** and **Table 2**). The AFM images of these films reveals the smooth surface patterns with root mean square (RMS)

roughness as small as ~0.40 nm, manifesting the uniform dispersion of ***x*PXZPO** in DPEPO matrixes. Therefore, in spite of various intermolecular interactions for ***x*PXZPO**, the employment of DPEPO as host can effectively suppress the aggregation and phase separation of ***x*PXZPO** to form the stable and uniform amorphous films.

3.3. Gaussian Simulations

Density function theory (DFT) and time-dependent DFT (TDDFT) calculations on ground (S_0) state and the first singlet (S_1) and triplet (T_1) excited states of ***x*PXZPO** were performed to figure out their frontier molecular orbital contributions (**Figure S2**), configuration stabilities and transition characteristics (**Figure 3**).

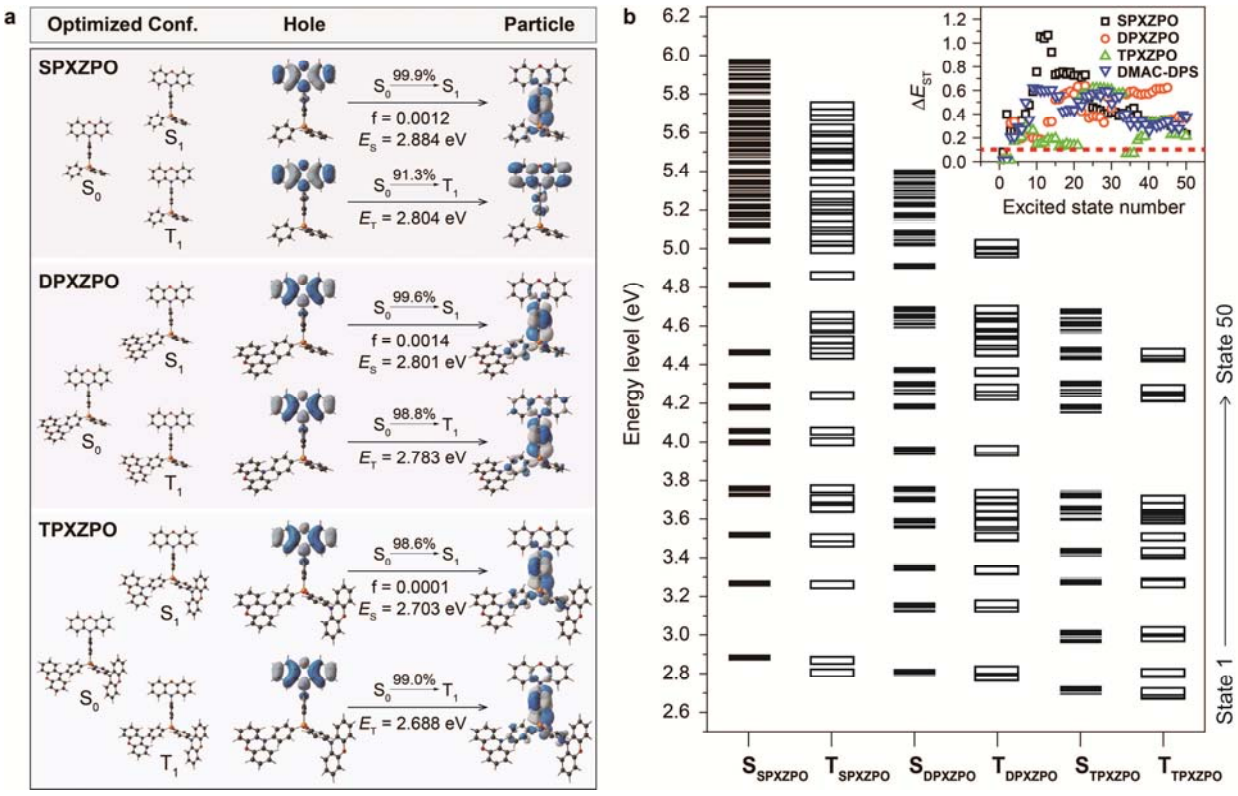

Figure 3. (a) Optimized molecular configurations of ***x*PXZPO** at S_0, S_1 and T_1 states and the natural orbital transition characteristics of their S_1 and T_1 states; (b) TDDFT calculated the

lowest 50 singlet and triplet energy levels of ***x*PXZPO** and the corresponding singlet-triplet splitting in comparison to **DMAC-DPS** (inset).

As designed, the HOMO, HOMO-1 and HOMO-2 of ***x*PXZPO** are thoroughly contributed by their phenoxazine groups; while, their LUMO, LUMO+1 and LUMO+2 are completely localized on their triphenylphosphine oxide (TPPO) groups, indicating the fully separated frontier molecular orbitals (FMO) (**Figure S2**). It is noteworthy that in contrast to **SPXZPO**, one more phenoxazine substituent in **DPXZPO** remarkably decreases its LUMO energy level by 0.2 eV; while, the tertiary phenoxazine renders the further LUMO reduction by 0.14 eV for **TPXZPO** (**Table 1**). In the meanwhile, ***x*TPXZPO** reveal the similar HOMO energy levels with negligible differences of ~0.06 eV. Consequently, the HOMO-LUMO energy gaps of ***x*PXZPO** are gradually shortened by 0.1-0.15 eV. Since phenoxazine is electron donor without any contributions to the unoccupied molecular orbitals and the number of P=O group in ***x*PXZPO** is the same, it is rational that the degressive LUMO energy levels of ***x*PXZPO** are due to the enhanced ICT in multi-dipolar structured analogues. Nevertheless, the spin density distributions (SDD) of the optimized T_1 states show the identical T_1 locations of ***x*PXZPO** on one of their *N*-phenyl-phenoxazine moieties, accompanied with the similar T_1 energy of ~2.75 eV, which should be attributed to the effectively suppressed conjugation extension and intramolecular electronic coupling by insulating effect of their P=O joints (**Figure S2**).

The configurations of ***x*PXZPO** in the S_0, S_1 and T_1 states are almost identical with the unchanged right dihedral angles between phenoxazines and *N*-phenyls and the similar geometries of P=O moieties, indicating the restrained excited-state structural relaxation, which is the combined result of the high rigidity of phenoxazine and the stable tetrahedral configuration of P=O (**Figure 3a**). TDDFT simulation was further performed to investigate the singlet and triplet

transition characteristics of ***x*PXZPO** with natural transition orbitals (NTO).[26] For $S_0 \rightarrow S_1$ excitations, ***x*PXZPO** show the CT-type transitions with identical "hole" and "particle" locations on phenoxazine and TPPO groups, respectively. NTOs of $S_0 \rightarrow T_1$ excitations for **DPXZPO** and **TPXZPO** reveal the same CT-characteristic transitions with "hole" and "particle" locations similar to their $S_0 \rightarrow S_1$ transitions. Contrarily, "hole" and "particle" of $S_0 \rightarrow T_1$ excitation for **SPXZPO** are overlapped on its phenoxazine, characteristic of locally excited (LE) state. In accordance with equation (1), the similar CT characteristics of singlet and triplet transitions give rise to the small ΔE_{ST} and therefore facilitate the $S_1 \leftrightarrow T_1$ conversions.[68]

Consistent with DFT results, the TDDFT-evaluated S_1 and T_1 energy of ***x*PXZPO** is also synchronously decreased. Nevertheless, **DPXZPO** and **TPXZPO** still achieve the S_1 energy of 2.8 and 2.7 eV for blue emission. Through increasing phenoxazine number, the ΔE_{ST} is successfully reduced from 0.08, 0.02 to 0.01 eV, further evidencing the effectiveness of multi-dipolar characteristics on the ICT enhancement. Noticeably, along with the extension of molecular system from **SPXZPO**, **DPXZPO** to **TPXZPO**, their excited state densities are remarkably increased, simultaneously reducing the singlet-triplet energy gaps between the S_n and T_n excited states (ΔE_{ST}^n) (**Figure 3b**). In contrast to **SPXZPO** with single one ΔE_{ST}^n (n = 1) less than 0.1 eV, **DPXZPO** reveals two singlet-triplet couples with $\Delta E_{ST}^n < 0.1$ eV (n = 1 and 2); while, as many as six singlet-triplet couples of **TPXZPO** achieve the negligible ΔE_{ST}^n within 0.1 eV (n = 1, 2, 3, 34, 35 and 36) as potential RISC channels (inset of **Figure 3b**).

On account of the similarity between singlet and triplet transitions for ***x*PXZPO** in the order of **TPXZPO**>**DPXZPO**>>**SPXZPO** and their ΔE_{ST} in the reverse order, the RISC of **TPXZPO** is doubtlessly the most efficient among ***x*PXZPO**, indicating the superiority of multi-dipolar

chromophores as blue TADF emitters on the basis of P=O joints with harmonious electron-withdrawing and insulating effects.

Table 1. Physical properties of ***x*PXZPO**.

Compound	$\lambda_{Abs.}$ (nm)	$\lambda_{Em.}$ (nm)	η_{PL}[c] (%)	S_1 (eV)	T_1 (eV)	ΔE_{ST} (eV)	f[h]	T_m/T_d (°C)	HOMO (eV)	LUMO (eV)	μ_h/μ_e[k] ($cm^2\ V^{-1}\ s^{-1}$)
SPXZPO	368, 323, 236[a]	467[a]	45[c]	2.99[d]	2.73[f]	0.26[g]	0.0012	228/370	-5.57[i]	-2.54[i]	1.8×10^{-7}
	381, 326, 240[b]	470[b]		2.88[e]	2.80[e]	0.08[e]			-4.69[j]	-1.10[j]	1.3×10^{-6}
DPXZPO	370, 323, 239[a]	471[a]	57[c]	2.92[d]	2.73[f]	0.19[g]	0.0014	240/440	-5.57[i]	-2.57[i]	7.4×10^{-5}
	389, 333, 243[b]	474[b]		2.80[e]	2.78[e]	0.02[e]			-4.76[j]	-1.30[j]	6.5×10^{-7}
TPXZPO	371, 322, 239[a]	474[a]	65[c]	2.84[d]	2.73[f]	0.11[g]	0.0001	302/459	-5.57[i]	-2.66[i]	7.7×10^{-5}
	385, 326, 243[b]	480[b]		2.70[e]	2.69[e]	0.01[e]			-4.82[j]	-1.48[j]	2.6×10^{-9}

[a] Absorption and Emission in toluene (10^{-6} mol L^{-1}); [b] absorption and Emission in film; [c] relative PLQY of degassed toluene solutions calculated by using 9,10-diphenylanthracene as standard; [d] estimated according to the absorption edges; [e] NTO calculated results; [f] calculated according to the 0-0 transitions of the phosphorescence spectra; [g] calculated according to the experimental values; [h] oscillator strength calculated with TDDFT method; [i] calculated according to the equation HOMO/LUMO = 4.78 + onset voltage; [j] DFT calculated results; [k] Zero-field hole and electron mobility evaluated by *I-V* characteristics of single carrier transporting devices with field-dependent space charge limited current (SCLC) model.

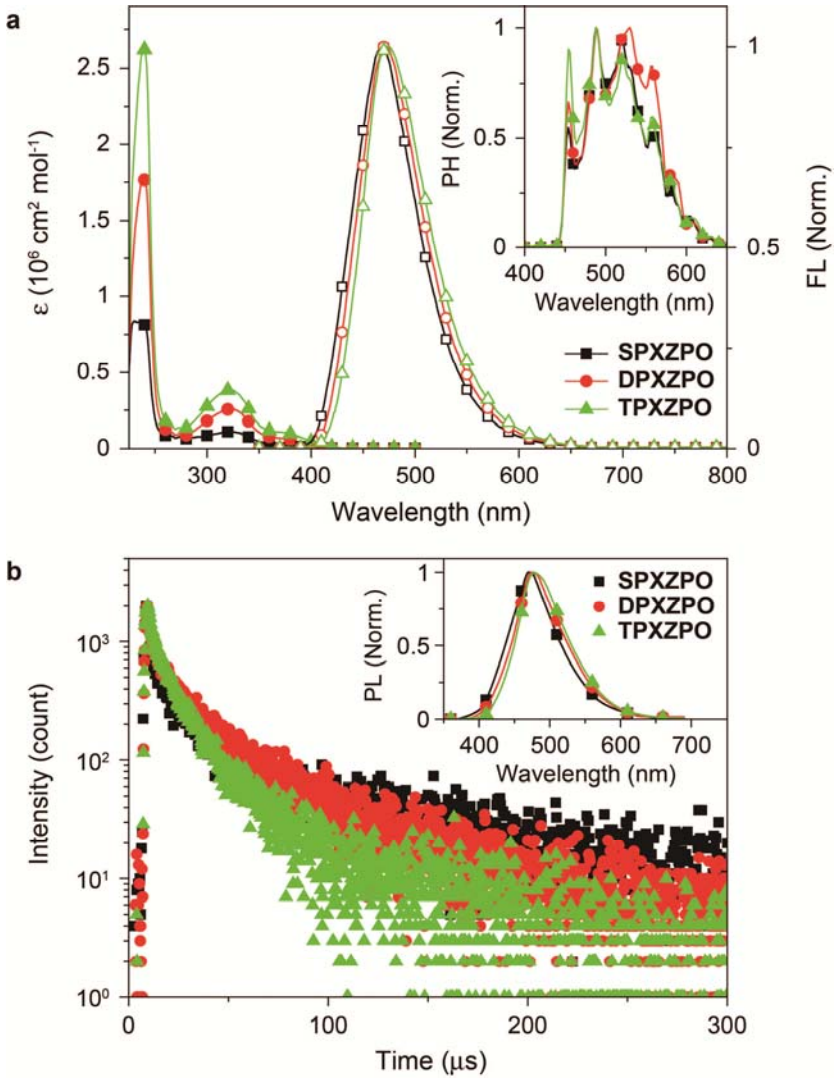

Figure 4. (a) Absorption, fluorescence (FL) and phosphorescence (PH) spectra in dilute toluene solutions (10^{-6} mol L^{-1}) of ***x*PXZPO**. PH spectra were measured with time-resolved technology after a delay of 300 μs; (b) Time decay curves and emission spectra (inset) of *vacuum*-evaporated ***x*PXZPO**:**DPEPO** films (10%wt., 100 nm).

3.4. Optical Properties

In dilute solutions (10^{-6} mol L^{-1} in degassed toluene), ***x*PXZPO** reveal the similar absorption spectra characteristic of three bands around 370, 320 and 240 nm, corresponding to $n \rightarrow \pi^*$

transition from phenoxazine to TPPO and $\pi \rightarrow \pi^*$ transitions of phenoxazine and phenyl, respectively (**Figure 4a**). The band intensities are in direct proportion to the absorption cross-sections of ***x*PXZPO**. Furthermore, from **SPXZPO**, **DPXZPO** to **TPXZPO**, their absorption edges shift bathochromicly, corresponding to their band-gap energy gradually decreased from 2.99, 2.92 to 2.84 eV, which is in exact accordance with TDDFT calculated results (**Table 1**). In virtue of the suppressed conjugation extension and intramolecular electronic interplays by P=O joints, ***x*PXZPO** successfully realize the blue fluorescence (FL) with peaks around 470 nm and bathochromic intervals less than 4 nm. The time decay curves at different temperature further reveal the distinct temperature-correlated lifetime variation, verifying the TADF-featured emissions from these P=O jointed D-A systems at room temperature (**Figure S3**). The CT characteristics of the S_1 states for ***x*PXZPO** were experimentally manifested by their strong solvatochromic effects with remarkable bathochromic shift beyond 100 nm along with solvent polarity increasing from toluene to methanol (**Figure S4**). The phosphorescence (PH) spectra of ***x*PXZPO** were measured at 77 K with time-resolved technology to get rid of the interference from FL (inset of **Figure 4a**). These spectra are extremely similar in wavelength range and profiles, attributed to the same T_1 locations of ***x*PXZPO** (**Figure S2**). According to 0→0 transitions, ***x*PXZPO** achieve the identical T_1 energy of 2.73 eV. Consequently, in accord with TDDFT simulated results, from **SPXZPO**, **DPXZPO** to **TPXZPO**, their ΔE_{ST} is remarkably decreased from 0.26, 0.19 to 0.11 eV, manifesting the predominance of multi-dipolar structure in facilitating RISC and realizing TADF. The difference between calculated and experimental values would be attributed to the underestimation on the basis of B3LYP, which can be further improved by employing other simulation methods, such as Tamm-Dancoff approximation (TDA).[69-70] The relative photoluminescence quantum yields (PLQY, η_{PL}) of ***x*PXZPO** are

evaluated as 45%, 57% and 65%, respectively, which are roughly in accord with their molecular rigidities and RISC efficiencies (**Table 1**). PLQYs of ***x*PXZPO** are comparable to those of their triazine congeners,[6] ascribed to the small oscillator strengths of their CT-characteristic transitions.

***x*PXZPO** were doped in DPEPO (10%wt.) to prepared the films through *vacuum* evaporation for optical analysis. All of these films emit blue light with the negligible bathochromic shift within 8 nm (inset of **Figure 4b** and **Table 2**). The absolute η_{PL} of **TPXZPO**-based films reaches to 67%, which is 12% and 25% higher than those of **DPXZPO** and **SPXZPO**-doped films, respectively. The PF lifetimes (τ_{PF}) of **SPXZPO**, **DPXZPO** and **TPXZPO** are gradually increased from 8, 13 to 20 ns. Contrarily, the order of DF lifetimes (τ_{DF}) for ***x*PXZPO** is reverse as 95, 31 and 17 μs, accompanied with gradually increased quantum yields (η_{DF}) of 36%, 45% and 51%, respectively. The reduced τ_{DF} benefits from the rapid RISC facilitated through decreasing ΔE_{ST}. The rate constants of PF and DF (k_{PF} and k_{DF}) can be evaluated according to experimental data[71]:

$$k_{PF} = \frac{\eta_{PF}}{\tau_{PF}} \tag{2}$$

$$k_{DF} = \frac{\eta_{DF}}{\tau_{DF}} \tag{3}$$

k_{PF} of ***x*PXZPO** are nearly the same by the order of 10^6 s^{-1}. In contrast, their k_{DF} are significantly differentiated. **TPXZPO** achieves the largest k_{DF} of 3.0×10^4 s^{-1}, which is 2 and 8 times of those of **DPXZPO** and **SPXZPO**, respectively (**Table 2**). It is showed that the differences in optical performances of ***x*PXZPO** are mainly attributed to their various delayed fluorescence behaviors. To figure out this issue, the rate constants of intersystem crossing (ISC) and RISC (k_{ISC} and k_{RISC}) are further estimated according to[2]:

$$k_{ISC} = \frac{\eta_{DF} \cdot k_{PF}}{\eta_{DF} + \eta_{PF}} \quad (4)$$

$$k_{RISC} = \frac{k_{DF} \cdot k_{PF} \cdot \eta_{DF}}{k_{ISC} \cdot \eta_{PF}} \quad (5)$$

$$k_{PF} = k_r^S + k_{nr}^S + k_{ISC} \quad (6)$$

It is interesting that ***x*PXZPO** reveal the almost identical k_{ISC} (**Table 2**). According to Equation (6), in which k_r^S and k_{nr}^S refer to radiative and nonradiative rate constant of singlet excited state, the singlet transition characteristics of ***x*PXZPO** are similar on the basis of their comparable $\left(k_r^S + k_{nr}^S\right)$, owing to the insulting effect of P=O joint on intramolecular interplays. On contrary, RISC of **TPXZPO** is dramatically facilitated with the remarkably improved k_{RISC} of 1.3×10^5 s^{-1}, which is 1.5 and 5 folds of those of **DPXZPO** and **SPXZPO**, respectively.

In consequence, the appropriate electron-withdrawing and insulating effects of P=O joint group are rationally utilized to preserve the blue emissions from multi-dipolar chromophores with strengthened ICT characteristics for RISC and TADF enhancement.

Table 2. Physical properties of ***x*PXZPO** doped in **DPEPO** films (10%wt.).

Compound	*RMS* (nm)	λ_{Em}[b] (nm)	η_{PL}[c] (%)	η_{PF}/η_{DF}[d] (%)	τ_{PF} (ns)	τ_{DF} (μs)	k_{PF} (10^6 s^{-1})	k_{DF} (10^3 s^{-1})	k_{ISC} (10^6 s^{-1})	k_{RISC} (10^4 s^{-1})
SPXZPO	0.37	470	42	6/36	8	95	7.5	3.8	6.4	2.7
DPXZPO	0.40	476	55	10/45	13	31	7.7	14.5	6.3	8.0
TPXZPO	0.38	478	67	16/51	20	17	8.0	30.0	6.1	12.5

[a] Root-mean-square surface roughness of *vacuum*-evaporated film (100 nm); [b] emission peak; [c] absolute PLQY measured with integrating sphere; [d] estimated according to the prompted and delayed proportions in transient decay curves.

3.5. Electrical Properties

When doped in relatively inert host matrixes, such as DPEPO, TADF dyes with ambipolar characteristics would make significant contributions to charge injection and transportation in emissive layers (EML) even at low doping concentrations.[72] In this case, the electrical performance of TADF dyes would influence the charge flux balance, carrier recombination efficiency and exciton quenching processes.

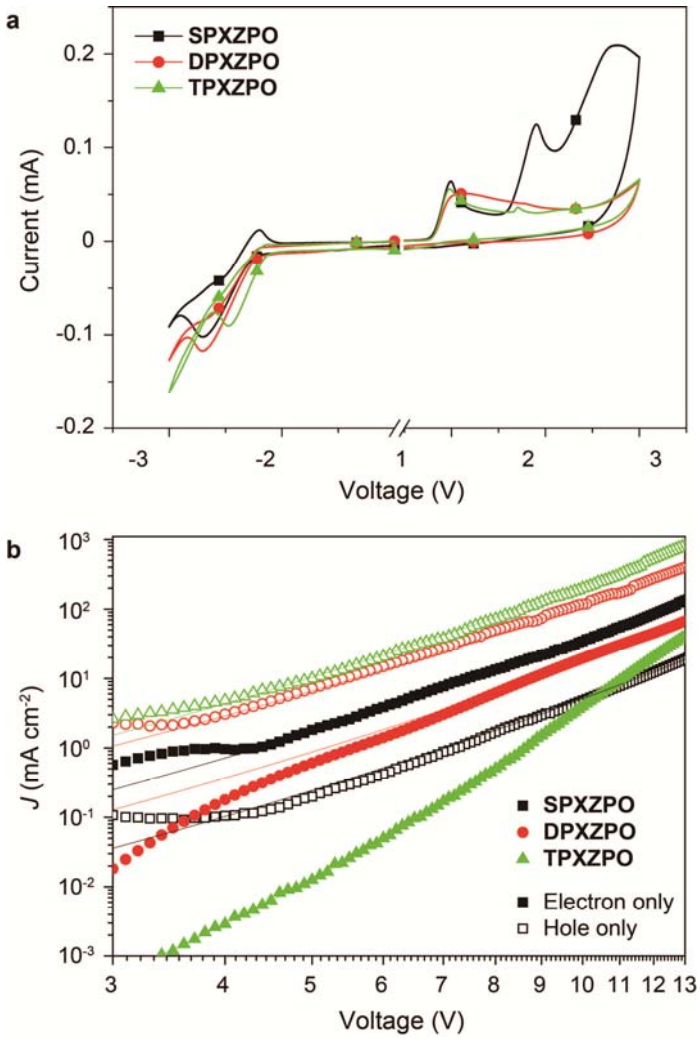

Figure 5. (a) Cyclic voltammograms of ***x*PXZPO** measured at room temperature with the scanning rate of 100 mV s^{-1}; (b) *I-V* characteristics of nominal single-carrier transporting devices based on ***x*PXZPO**.

The cyclic voltammetry (CV) analysis of ***x*PXZPO** was performed to experimentally determine their FMO energy levels, according to the electron gain and loss processes (**Figure 5a**). **SPXZPO** reveals three irreversible anodic peaks, of which the first two correspond to the oxidation of phenoxazine and the third one originates from DPPO, respectively. The phenoxazine-attributed anodic peaks of **DPXZPO** and **TPXZPO** are remarkably broadened due to their more phenoxazine groups. Nevertheless, the onset voltages of these oxidation curves are the same as 0.79 V, corresponding to the HOMO of -5.57 eV. Contrarily, the reduction curves of ***x*PXZPO** consist of one quasi-reversible cathodic peak with gradually increased onset voltages from -2.24, -2.21 to -2.12 V, corresponding to the LUMO of -2.54, -2.57 and -2.66 eV, respectively. In contrast to the experimental values, the smaller differences of the theoretical values should be attributed to the ignored insulating effect of P=O joint in controlling intramolecular interplays. Nevertheless, the reduced HOMO-LUMO energy gaps of ***x*PXZPO** are consistent with DFT simulation as the result of enhanced ICT in the multi-dipolar structures. In consideration of the HOMO an LUMO for DPEPO as -6.5 and -2.5 eV, **TPXZPO** can form the hole and electron traps with depths about 0.9 and 0.2 eV, respectively, for direct carrier and exciton capture, which would be beneficial to reduce energy loss during host-dopant energy transfer.[50]

The nominal single-carrier transporting devices for ***x*PXZPO** with configuration of ITO|LiF (1 nm)| ***x*PXZPO** (100 nm)|LiF (1 nm)|Al for electron only and ITO|MoO_3 (6 nm)| ***x*PXZPO** (100 nm)|MoO_3 (6 nm)|Al for hole only were fabricated to evaluate their carrier transporting abilities, in which LiF and MoO_3 were used as hole- and electron-injecting layers, respectively (**Figure 5b**). It was showed that the hole-only current densities (*J*) of these devices were in direct proportion to the number of phenoxazine groups in ***x*PXZPO**, while just the opposite for

electron-only *J*. Because phenoxazine and TPPO groups respectively establish the hole and electron transporting channels in ***x*PXZPO**, it is rational that the increase of peripheral phenoxazine groups can facilitate the hole hopping between adjacent molecules and simultaneously impede the electron migration due to the encapsulation and isolation of TPPO groups. According to filed-dependent space charge limited current (SCLC) model, the zero-field hole and electron mobilities (μ_h and μ_e) of ***x*PXZPO** are estimated as 1.8×10^{-7}, 7.4×10^{-5} and 7.7×10^{-5} cm^2 V^{-1} s^{-1} and 1.3×10^{-6}, 6.5×10^{-7} and 2.6×10^{-9} cm^2 V^{-1} s^{-1}, respectively. Therefore, the carrier transporting characteristics of ***x*PXZPO** change from electron-predominant transportation of **SPXZPO** to hole-predominant transportation of **DPXZPO** and **TPXZPO**. Nevertheless, the drawback of **TPXZPO** in charge flux balance can be partially remedied through employing the electron-transporting host materials, such as DPEPO.

3.6. EL Performance

The achievement and enhancement of blue TADF emissions by multi-dipolar WASD-type ***x*PXZPO** encouraged us to fabricate their organic light-emitting diodes (OLED) with configuration of ITO|MoO_3 (6 nm)|NPB (70 nm)|*m*CP (5 nm)|DPEPO:***x*PXZPO** (20 nm, 10%wt.)|DPEPO (5 nm)|Bphen (30 nm)|LiF (1 nm)|Al, in which 4,4'-bis[*N*-(1-naphthyl)-*N*-phenylamino]biphenyl (NPB) and 4,7-diphenyl-1,10-phenanthroline (Bphen) were used as hole and electron transporting layers, while *N*,*N*'-dicarbazole-3,5-benzene (*m*CP) and DPEPO were used as exciton blocking layers, respectively (**Figure 6a**). The most popular SAWD-type blue TADF dye bis[4-(9,9-dimethyl-9,10-dihydroacridine)phenyl]sulfone (DMAC-DPS)[21, 23] was also adopted to fabricate the control devices for comparison.

EL spectra of these devices consisted of the pure emissions from the TADF dyes (**Figure 6b**). **SPXZPO**-based devices achieved the EL emissions with the peaks at 448 nm and CIE

coordinates as small as (0.16, 0.12), corresponding to the deep-blue light with $x+y<0.3$ (**Table 3**). **DPXZPO** supported its devices with the blue emissions with the peaks at 460 nm and CIE coordinates of (0.16, 0.20), which were identical to the DMAC-DPS-based devices. Nevertheless, it is noteworthy that there were more blue components in EL emissions of **DPXZPO**-based devices. Similar to the situation of PL, **TPXZPO** successfully realized the pure-blue EL emission peaked at 464 nm with negligible bathochromic shift of only 4 nm in comparison to **DPXZPO**, accompanied by the favorable CIE coordinates of (0.17, 0.20).

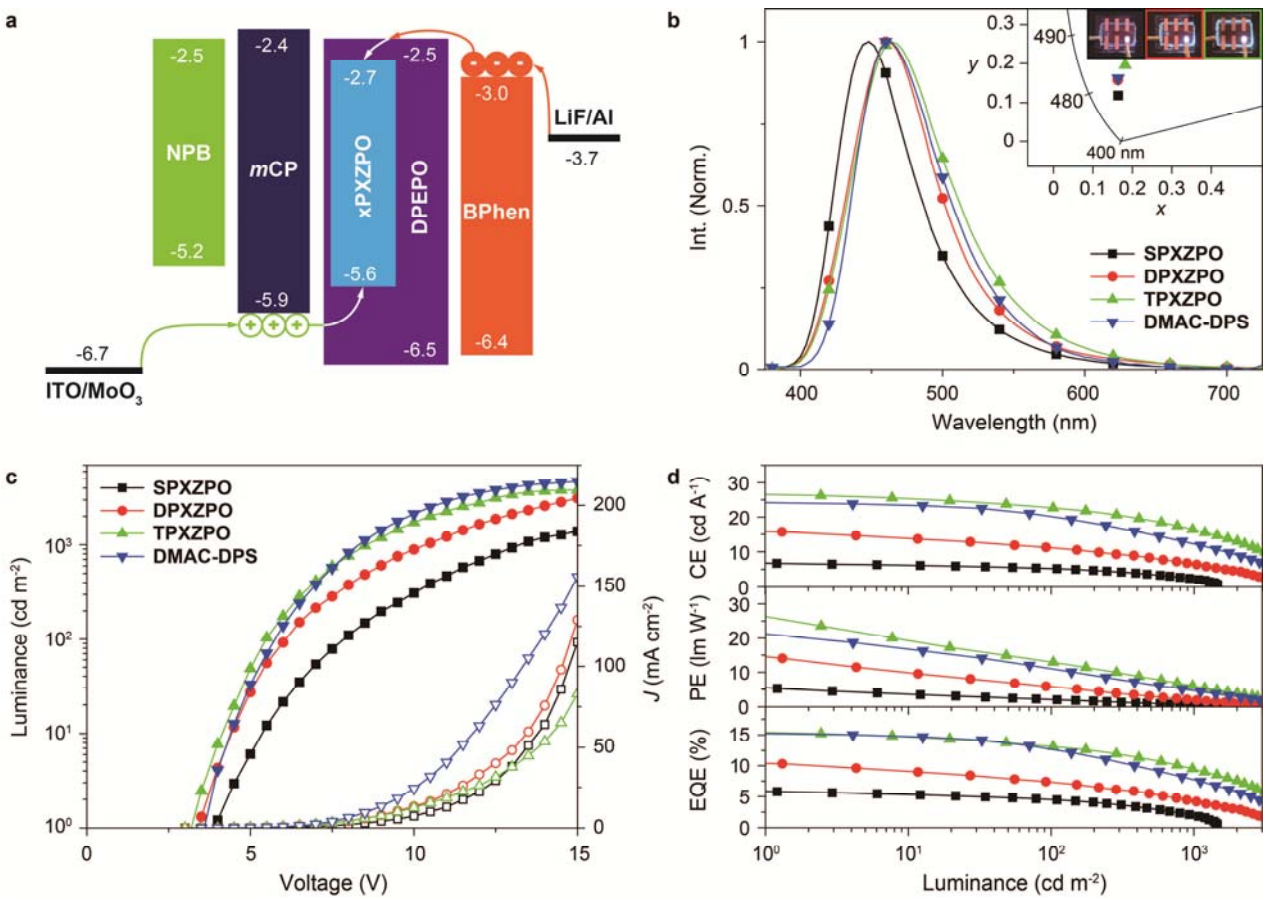

Figure 6. EL performance of ***x*PXZPO** as blue emitters. (a) Device structure and energy level diagram; (b) EL spectra and device photos at 5 V; (c) luminance-current density (*J*)-voltage curves; (d) efficiencies-luminance curves.

TPXZPO endowed its devices with the lowest driving voltages of 3.5, <5.5 and <9.0 V for onset and at 100 and 1000 cd m^{-2}, respectively (**Figure 6c** and **Table 3**). **DPXZPO**-based devices achieved the comparable onset voltage, but their driving voltages remarkably rose by >1 V at 100 and 1000 cd m^{-2}. The driving voltages of **SPXZPO**-based devices further increased to 4, <7.5 and <13.5 V for onset and at 100 and 1000 cd m^{-2}, respectively. It is showed that the driving voltages of these devices were exactly consistent with the LUMO energy levels of their emitters, manifesting the significant involvement of ***x*PXZPO** in carrier injection of EMLs. Therefore, it is rational that the dominant EL mechanism of these devices should be the direct carrier and exciton capture by ***x*PXZPO**, which is similar to DMAC-DPS-based devices. Notably, **TPXZPO** realized the driving voltages almost equivalent, even partially lower, to those of DMAC-DPS-based control devices, owing to the intrinsic advantage of its WASD-type and multi-dipolar structure in carrier injection enhancement.

TPXZPO-based devices realized the favorable efficiencies with the maxima of 26.4 cd A^{-1} for current efficiency (CE), 23.6 lm W^{-1} for power efficiency (PE) and 15.3% for η_{ext}, accompanied by the reduced EQE roll-offs of 14% and 41% at 100 and 1000 cd m^{-2}, respectively (**Figure 6d** and **Table 3**). Besides of the improved efficiency stability, the maximum η_{ext} of **TPXZPO**-based devices were 1.5 and 2.5 times of those of **DPXZPO** and **SPXZPO**-based analogues. Assuming outcoupling efficiency for ITO glass substrates as 25±5% and hole-electron recombination ratio as 1, the maximum exciton utilization efficiency of **TPXZPO**-based devices reached to 95±19%, remarkably higher than 80±16% and 63±12% for **DPXZPO** and **SPXZPO**-based analogues. Obviously, the highest EL efficiencies of **TPXZPO** among ***x*PXZPO** should be mainly attributed to its optimal TADF performance owing to its multi-dipolar characteristics.

It is showed that on the basis of the same device configuration, **TPXZPO** achieves the EL performance comparable to those of DMAC-DPS, indicating the effectiveness of WASD strategy in constructing high-performance blue TADF dyes. Despite the remarkably longer emission lifetime and lower PLQY of **TPXZPO** than those of DMAC-DPS (τ_{DF} = 3 μs, η_{PL} = 90% in DPEPO)[23], **TPXZPO** instead realized the preserved EL efficiencies and the reduced efficiency roll-offs, which should be attributed to the improved charge flux balance in the EML with complementation of hole-predominant **TPXZPO** and electron-predominant DPEPO, verifying the predominance of multi-dipolar configuration in exciton utilization and quenching suppression.

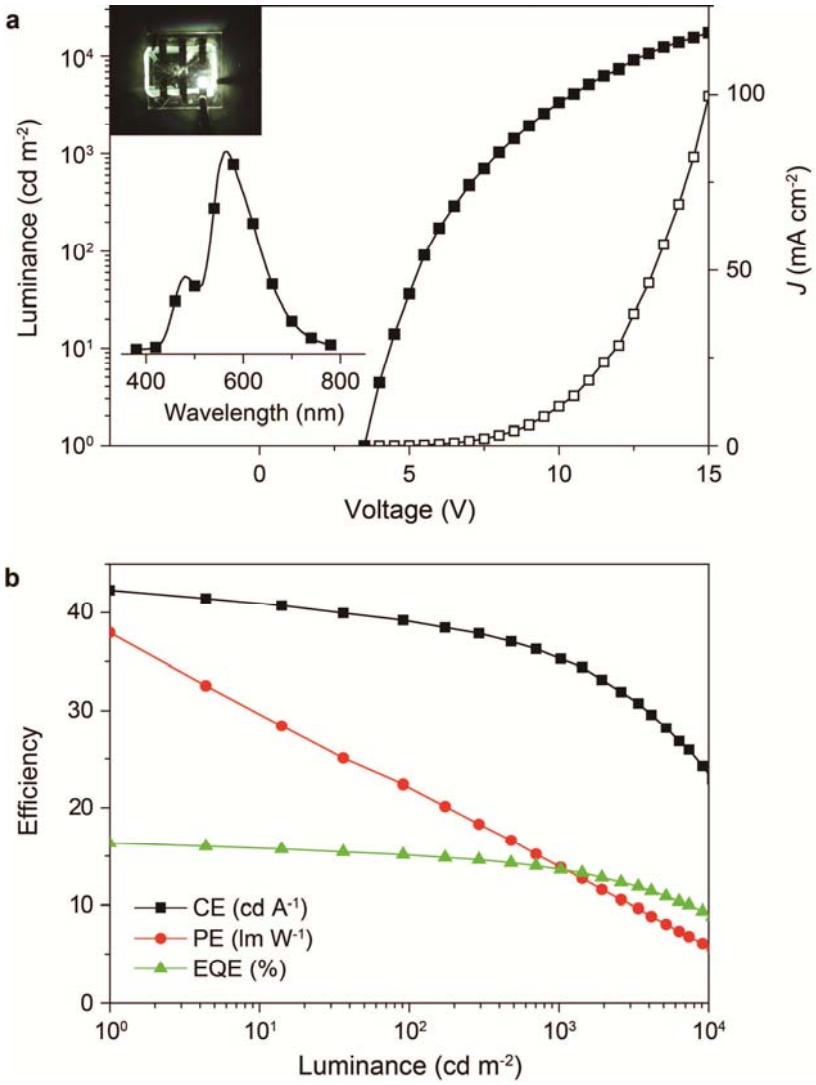

Figure 7. EL performance of complementary WOLEDs using **TPXZPO** as blue emitter. (a) Luminance-*J*-voltage curves, EL spectrum and device photo at 500 cd m^{-2} (inset); (b) efficiencies-luminance curves.

We further used a universal host 4'-diphenylphosphinoylspiro[fluorene-9,9'-xanthene] (SFXSPO)[73] to fabricate the complementary full-TADF white devices with a bi-EML configuration of ITO|MoO_3 (6 nm)|NPB (70 nm)|*m*CP (5 nm)|SFXSPO:4CzPNPh (20 nm, 5%wt.)|SFXSPO:**TPXZPO** (20 nm, 10%wt.)|SFXSPO (5 nm)|Bphen (30 nm)|LiF (1 nm)|Al, in which **TPXZPO** and 3,4,5,6-tetrakis(3,6-diphenylcarbazol-9-yl)-1,2-dicyanobenzene (4CzPNPh) served as blue and yellow TADF dopants, respectively (**Scheme S1**). At 500 cd m^{-2}, the warm-white emission was successfully achieved with two peaks at 484 and 556 nm, originated from **TPXZPO** and 4CzPNPh, respective, and favorable CIE coordinates of (0.42, 0.45), which was close to the warm-white standard illuminant A (0.45, 0.41) defined by the CIE 1931 chromaticity coordinate system (inset of **Figure 7a**). The devices showed the relatively low driving voltages of 3.5, <6.0 and <8.0 V for onset and at 100 and 1000 cd m^{-2}, respectively, and the maximum luminance beyond 20000 cd m^{-2} (**Figure 7a** and **Table 3**). Furthermore, the high efficiencies were realized with the maxima of 42.3 cd A^{-1}, 38.0 lm W^{-1} and 16.3%, corresponding to a favorable η_{int} of ~50-80%, which are comparable to the best results of full-TADF WOLEDs (**Figure 7b** and **Table 3**).[73]

The success of **TPXZPO** in blue and white TADF diodes with impressive EL performance should originates from its balance and harmonious optoelectronic properties, manifesting the merits of WASD systems as blue emitters characteristic of substantially adjustable ICT for electrical performance optimization and TADF enhancement.

Table 3. EL performance of the blue and white TADF diodes.

Host	TADF Dye	λ_{Em} (nm)	Operating Voltage[a] (V)	Maximum Efficiencies[b]	Efficiency Roll-Offs[c] (%)			CIE (x, y)
					C.E.	P.E.	E.Q.E.	
Blue TADF Devices								
DPEPO	**DMAC-DPS**	460	<4, <6.0, <8.5	24.2, 21.7, 15.2	20, 51	54, 80	20, 51	0.16, 0.17
	SPXZPO	448	4, <7.5, <13.5	7.3, 7.6, 6.3	29, 71	73, 94	29, 71	0.16, 0.12
	DPXZPO	460	3.5, <6.5, <10.5	16.1, 16.9, 10.6	33, 59	64, 86	33, 59	0.16, 0.17
	TPXZPO	464	3.5, <5.5, <9.0	26.4, 23.6, 15.3	14, 41	45, 77	14, 41	0.17, 0.20
White TADF Devices								
SFXSPO	**DMAC-DPS /4CzPNPh**[73]	484/556	3.9, <5.5, <7.3	50.5, 40.6, 19.1	4, 18	32, 56	4, 18	0.32, 0.43
	TPXZPO/4CzPNPh	480/564	3.5, <6.0, <8.0	42.3, 38.0, 16.3	9, 17	47, 64	9, 17	0.42, 0.45

[a] In the order of onset, 100 and 1000 cd m^{-2}; [b] in the order of CE (cd A^{-1}), PE (lm W^{-1}) and EQE (%); [c] in the order of 100 and 1000 cd m^{-2}.

4. Conclusions

A series of WASD-type emitters named ***x*PXZPO** were prepared with P=O as acceptor and joint group. The multi-dipolar chromophore **TPXZPO** successfully realizes the preserved blue emission, owing to the insulating effect of P=O joint on conjugation extension and intramolecular electron communication. Simultaneously, its multiple ICT remarkably facilitates RISC with reduced ΔE_{ST} of ~0.1 eV, supporting the efficient TADF emission with higher PLQY and shorter lifetime. As the result, **TPXZPO** endowed its devices with the pure-blue EL emission with favorable CIE coordinates of (0.17, 0.20) and impressive η_{ext} up to 15.3%, corresponding to the maximum exciton utilization efficiency of ~100%. With **TPXZPO** as blue emitter, the white full-TADF diodes achieved the maximum η_{ext} of 16.3%. It is showed that the

employment of P=O with combined electron-withdrawing and insulating effects is the key to successfully construct the blue-emitting multi-dipolar chromophore, which establishes a solid example of high-efficiency WASD-type blue TADF dyes as a feasible and prepotent strategy. Nevertheless, EL efficiency of **TPXZPO** is still limited by its moderate PLQY, which can be improved through further enhancing structural rigidity and tuning the D-A interactions. The subsequent modification is already under way in our laboratory.

ASSOCIATED CONTENT

Supporting Information. Thermal properties, energy levels and contours of FMOs and spin-density distributions of the T_1 states and emission dependence on temperature and solvent polarity of ***x*PXZPO** and device structure and chemical structures of employed materials for white OLEDs.

AUTHOR INFORMATION

Corresponding Author

hxu@hlju.edu.cn

Author Contributions

‡These authors contributed equally.

ACKNOWLEDGMENT

CD and JL contributed equally to this work. This project was financially supported by NSFC (51373050), New Century Excellent Talents Supporting Program of MOE (NCET-12-0706), Science and Technology Bureau of Heilongjiang Province (ZD201402 and JC2015002), Education Bureau of Heilongjiang Province (2014CJHB005), the Fok Ying-Tong Education

Foundation for Young Teachers in the Higher Education Institutions of China (141012) and

Harbin Science and Technology Bureau (2015RAYXJ008).

REFERENCES

1. Endo, A.; Ogasawara, M.; Takahashi, A.; Yokoyama, D.; Kato, Y.; Adachi, C., Thermally Activated Delayed Fluorescence from Sn4+-Porphyrin Complexes and Their Application to Organic Light-Emitting Diodes - A Novel Mechanism for Electroluminescence. *Adv. Mater.* **2009,** 21, 4802-4806.
2. Uoyama, H.; Goushi, K.; Shizu, K.; Nomura, H.; Adachi, C., Highly efficient organic light-emitting diodes from delayed fluorescence. *Nature* **2012,** 492, 234-238.
3. Tao, Y.; Yuan, K.; Chen, T.; Xu, P.; Li, H.; Chen, R.; Zheng, C.; Zhang, L.; Huang, W., Thermally Activated Delayed Fluorescence Materials Towards the Breakthrough of Organoelectronics. *Adv. Mater.* **2014,** 26, 7931-7958.
4. Nakanotani, H.; Higuchi, T.; Furukawa, T.; Masui, K.; Morimoto, K.; Numata, M.; Tanaka, H.; Sagara, Y.; Yasuda, T.; Adachi, C., High-efficiency organic light-emitting diodes with fluorescent emitters. *Nat Commun* **2014,** 5, 4016.
5. Li, W.; Liu, D.; Shen, F.; Ma, D.; Wang, Z.; Feng, T.; Xu, Y.; Yang, B.; Ma, Y., A Twisting Donor-Acceptor Molecule with an Intercrossed Excited State for Highly Efficient, Deep-Blue Electroluminescence. *Adv. Funct. Mater.* **2012,** 22, 2797-2803.
6. Tanaka, H.; Shizu, K.; Nakanotani, H.; Adachi, C., Twisted Intramolecular Charge Transfer State for Long-Wavelength Thermally Activated Delayed Fluorescence. *Chem. Mater.* **2013,** 25, 3766-3771.
7. Park, Y.-S.; Kim, K.-H.; Kim, J.-J., Efficient triplet harvesting by fluorescent molecules through exciplexes for high efficiency organic light-emitting diodes. *Appl. Phys. Lett.* **2013,** 102, 153306.
8. Chen, X.-L.; Yu, R.; Zhang, Q.-K.; Zhou, L.-J.; Wu, X.-Y.; Zhang, Q.; Lu, C.-Z., Rational Design of Strongly Blue-Emitting Cuprous Complexes with Thermally Activated Delayed Fluorescence and Application in Solution-Processed OLEDs. *Chem. Mater.* **2013,** 25, 3910-3920.
9. Peng, Q. M.; Li, W. J.; Zhang, S. T.; Chen, P.; Li, F.; Ma, Y. G., Evidence of the Reverse Intersystem Crossing in Intra-Molecular Charge-Transfer Fluorescence-Based Organic Light-Emitting Devices Through Magneto-Electroluminescence Measurements. *Adv. Opt. Mater.* **2013,** 1, 362-366.
10. Milián-Medina, B.; Gierschner, J., Computational design of low singlet–triplet gap all-organic molecules for OLED application. *Org. Electron.* **2012,** 13, 985-991.
11. Huang, S.; Zhang, Q.; Shiota, Y.; Nakagawa, T.; Kuwabara, K.; Yoshizawa, K.; Adachi, C., Computational Prediction for Singlet- and Triplet-Transition Energies of Charge-Transfer Compounds. *J. Chem. Theory Comput.* **2013,** 9, 3872-3877.
12. Jankus, V.; Data, P.; Graves, D.; McGuinness, C.; Santos, J.; Bryce, M. R.; Dias, F. B.; Monkman, A. P., Highly Efficient TADF OLEDs: How the Emitter–Host Interaction Controls Both the Excited State Species and Electrical Properties of the Devices to Achieve Near 100% Triplet Harvesting and High Efficiency. *Adv. Funct. Mater.* **2014,** 24, 6178-6186.

13. Kim, B. S.; Lee, J. Y., Engineering of Mixed Host for High External Quantum Efficiency above 25% in Green Thermally Activated Delayed Fluorescence Device. *Adv. Funct. Mater.* **2014,** 24, 3970-3977.
14. Cho, Y. J.; Yook, K. S.; Lee, J. Y., A universal host material for high external quantum efficiency close to 25% and long lifetime in green fluorescent and phosphorescent OLEDs. *Adv. Mater.* **2014,** 26, 4050-5.
15. Wang, H.; Xie, L.; Peng, Q.; Meng, L.; Wang, Y.; Yi, Y.; Wang, P., Novel Thermally Activated Delayed Fluorescence Materials–Thioxanthone Derivatives and Their Applications for Highly Efficient OLEDs. *Adv. Mater.* **2014,** 26, 5198-5204.
16. Xie, G.; Li, X.; Chen, D.; Wang, Z.; Cai, X.; Chen, D.; Li, Y.; Liu, K.; Cao, Y.; Su, S.-J., Evaporation- and Solution-Process-Feasible Highly Efficient Thianthrene-9,9′,10,10′-Tetraoxide-Based Thermally Activated Delayed Fluorescence Emitters with Reduced Efficiency Roll-Off. *Adv. Mater.* **2016,** 28, 181-187.
17. Kim, M.; Jeon, S. K.; Hwang, S.-H.; Lee, J. Y., Stable Blue Thermally Activated Delayed Fluorescent Organic Light-Emitting Diodes with Three Times Longer Lifetime than Phosphorescent Organic Light-Emitting Diodes. *Adv. Mater.* **2015,** 27, 2515-2520.
18. Lee, D. R.; Kim, M.; Jeon, S. K.; Hwang, S.-H.; Lee, C. W.; Lee, J. Y., Design Strategy for 25% External Quantum Efficiency in Green and Blue Thermally Activated Delayed Fluorescent Devices. *Adv. Mater.* **2015,** 27, 5861-5867.
19. Hirata, S.; Sakai, Y.; Masui, K.; Tanaka, H.; Lee, S. Y.; Nomura, H.; Nakamura, N.; Yasumatsu, M.; Nakanotani, H.; Zhang, Q.; Shizu, K.; Miyazaki, H.; Adachi, C., Highly efficient blue electroluminescence based on thermally activated delayed fluorescence. *Nat. Mater.* **2015,** 14, 330-336.
20. Rajamalli, P.; Senthilkumar, N.; Gandeepan, P.; Huang, P.-Y.; Huang, M.-J.; Ren-Wu, C.-Z.; Yang, C.-Y.; Chiu, M.-J.; Chu, L.-K.; Lin, H.-W.; Cheng, C.-H., A New Molecular Design Based on Thermally Activated Delayed Fluorescence for Highly Efficient Organic Light Emitting Diodes. *J. Am. Chem. Soc.* **2016,** 138, 628-634.
21. Zhang, Q.; Tsang, D.; Kuwabara, H.; Hatae, Y.; Li, B.; Takahashi, T.; Lee, S. Y.; Yasuda, T.; Adachi, C., Nearly 100% Internal Quantum Efficiency in Undoped Electroluminescent Devices Employing Pure Organic Emitters. *Adv. Mater.* **2015,** 27, 2096-2100.
22. Lee, S. Y.; Yasuda, T.; Yang, Y. S.; Zhang, Q.; Adachi, C., Luminous Butterflies: Efficient Exciton Harvesting by Benzophenone Derivatives for Full-Color Delayed Fluorescence OLEDs. *Angew. Chem. Int. Ed.* **2014,** 53, 6402-6406.
23. Zhang, Q.; Li, B.; Huang, S.; Nomura, H.; Tanaka, H.; Adachi, C., Efficient blue organic light-emitting diodes employing thermally activated delayed fluorescence. *Nat. Photon.* **2014,** 8, 326-332.
24. Becke, A. D., Density-functional thermochemistry. III. The role of exact exchange. *J. Chem. Phys.* **1993,** 98, 5648-5652.
25. Lee, C.; Yang, W.; Parr, R. G., Development of the Colle-Salvetti correlation-energy formula into a functional of the electron density. *Phys. Rev. B* **1988,** 37, 785-789.
26. Martin, R. L., Natural transition orbitals. *J. Chem. Phys.* **2003,** 118, 4775-4777.
27. Frisch, M. J.; Trucks, G. W.; Schlegel, H. B.; Scuseria, G. E.; Robb, M. A.; Cheeseman, J. R.; Scalmani, G.; Barone, V.; Mennucci, B.; Petersson, G. A.; Nakatsuji, H.; Caricato, M.; Li, X.; Hratchian, H. P.; Izmaylov, A. F.; Bloino, J.; Zheng, G.; Sonnenberg, J. L.; Hada, M.; Ehara, M.; Toyota, K.; Fukuda, R.; Hasegawa, J.; Ishida, M.; Nakajima, T.; Honda, Y.; Kitao, O.; Nakai, H.; Vreven, T.; Montgomery, J. A.; Peralta, J. E.; Ogliaro, F.; Bearpark, M.; Heyd, J. J.; Brothers, E.;

Kudin, K. N.; Staroverov, V. N.; Kobayashi, R.; Normand, J.; Raghavachari, K.; Rendell, A.; Burant, J. C.; Iyengar, S. S.; Tomasi, J.; Cossi, M.; Rega, N.; Millam, J. M.; Klene, M.; Knox, J. E.; Cross, J. B.; Bakken, V.; Adamo, C.; Jaramillo, J.; Gomperts, R.; Stratmann, R. E.; Yazyev, O.; Austin, A. J.; Cammi, R.; Pomelli, C.; Ochterski, J. W.; Martin, R. L.; Morokuma, K.; Zakrzewski, V. G.; Voth, G. A.; Salvador, P.; Dannenberg, J. J.; Dapprich, S.; Daniels, A. D.; Farkas, Ö.; Foresman, J. B.; Ortiz, J. V.; Cioslowski, J.; Fox, D. J. Gaussian 09, Revision D. 1, Gaussian, Inc., Wallingford CT, USA: 2009.

28. Wu, C.-L.; Chang, C.-H.; Chang, Y.-T.; Chen, C.-T.; Chen, C.-T.; Su, C.-J., High efficiency non-dopant blue organic light-emitting diodes based on anthracene-based fluorophores with molecular design of charge transport and red-shifted emission proof. *J. Mater. Chem. C* **2014,** 2, 7188-7200.

29. Liu, C.; Li, Y.; Li, Y.; Yang, C.; Wu, H.; Qin, J.; Cao, Y., Efficient Solution-Processed Deep-Blue Organic Light-Emitting Diodes Based on Multibranched Oligofluorenes with a Phosphine Oxide Center. *Chem. Mater.* **2013,** 25, 3320-3327.

30. Chien, C.-H.; Chen, C.-K.; Hsu, F.-M.; Shu, C.-F.; Chou, P.-T.; Lai, C.-H., Multifunctional Deep-Blue Emitter Comprising an Anthracene Core and Terminal Triphenylphosphine Oxide Groups. *Adv. Funct. Mater.* **2009,** 19, 560-566.

31. Han, C.; Zhao, F.; Zhang, Z.; Zhu, L.; Xu, H.; Li, J.; Ma, D.; Yan, P., Constructing Low-Triplet-Energy Hosts for Highly Efficient Blue PHOLEDs: Controlling Charge and Exciton Capture in Doping Systems. *Chem. Mater.* **2013,** 25, 4966-4976.

32. Yu, D.; Zhao, F.; Zhang, Z.; Han, C.; Xu, H.; Li, J.; Ma, D.; Yan, P., Insulated donor-[small pi]-acceptor systems based on fluorene-phosphine oxide hybrids for non-doped deep-blue electroluminescent devices. *Chem. Commun.* **2012,** 48, 6157-6159.

33. Liu, X.-K.; Zheng, C.-J.; Lo, M.-F.; Xiao, J.; Lee, C.-S.; Fung, M.-K.; Zhang, X.-H., A multifunctional phosphine oxide-diphenylamine hybrid compound as a high performance deep-blue fluorescent emitter and green phosphorescent host. *Chem. Commun.* **2014,** 50, 2027-2029.

34. Lee, J.-H.; Cheng, S.-H.; Yoo, S.-J.; Shin, H.; Chang, J.-H.; Wu, C.-I.; Wong, K.-T.; Kim, J.-J., An Exciplex Forming Host for Highly Efficient Blue Organic Light Emitting Diodes with Low Driving Voltage. *Adv. Funct. Mater.* **2015,** 25, 361-366.

35. Jiang, W.; Xu, H.; Ban, X.; Yuan, G.; Sun, Y.; Huang, B.; Duan, L.; Qiu, Y., Alcohol-Soluble Electron-Transport Small Molecule for Fully Solution-Processed Multilayer White Electrophosphorescent Devices. *Org. Lett.* **2014,** 16, 1140-1143.

36. Gong, S.; Chang, Y.-L.; Wu, K.; White, R.; Lu, Z.-H.; Song, D.; Yang, C., High-Power-Efficiency Blue Electrophosphorescence Enabled by the Synergistic Combination of Phosphine-Oxide-Based Host and Electron-Transporting Materials. *Chem. Mater.* **2014,** 26, 1463-1470.

37. Jeon, S. O.; Yook, K. S.; Joo, C. W.; Lee, J. Y., A phosphine oxide derivative as a universal electron transport material for organic light-emitting diodes. *J. Mater. Chem.* **2009,** 19, 5940-5944.

38. Ha, M.-Y.; Moon, D.-G., Low voltage organic light-emitting devices with triphenylphosphine oxide layer. *Appl. Phys. Lett.* **2008,** 93, 043306.

39. Oyamada, T.; Sasabe, H.; Adachi, C.; Murase, S.; Tominaga, T.; Maeda, C., Extremely low-voltage driving of organic light-emitting diodes with a Cs-doped phenyldipyrenylphosphine oxide layer as an electron-injection layer. *Appl. Phys. Lett.* **2005,** 86, 033503-3.

40. Kan, W.; Zhu, L.; Wei, Y.; Ma, D.; Sun, M.; Wu, Z.; Huang, W.; Xu, H., Phosphine oxide-jointed electron transporters for the reduction of interfacial quenching in highly efficient blue PHOLEDs. *J. Mater. Chem. C* **2015,** 3, 5430-5439.

41. Jia, J.; Zhu, L.; Wei, Y.; Wu, Z.; Xu, H.; Ding, D.; Chen, R.; Ma, D.; Huang, W., Triazine-phosphine oxide electron transporter for ultralow-voltage-driven sky blue PHOLEDs. *J. Mater. Chem. C* **2015,** 3, 4890-4902.
42. Fan, C.; Duan, C.; Wei, Y.; Ding, D.; Xu, H.; Huang, W., Dibenzothiophene-Based Phosphine Oxide Host and Electron-Transporting Materials for Efficient Blue Thermally Activated Delayed Fluorescence Diodes through Compatibility Optimization. *Chem. Mater.* **2015,** 27, 5131-5140.
43. Ding, L.; Dong, S.-C.; Jiang, Z.-Q.; Chen, H.; Liao, L.-S., Orthogonal Molecular Structure for Better Host Material in Blue Phosphorescence and Larger OLED White Lighting Panel. *Adv. Funct. Mater.* **2015,** 25, 645-650.
44. Wang, K.; Wang, S.; Wei, J.; Chen, S.; Liu, D.; Liu, Y.; Wang, Y., New multifunctional phenanthroimidazole-phosphine oxide hybrids for high-performance red, green and blue electroluminescent devices. *J. Mater. Chem. C* **2014,** 2, 6817-6826.
45. Liu, H.; Bai, Q.; Yao, L.; Hu, D.; Tang, X.; Shen, F.; Zhang, H.; Gao, Y.; Lu, P.; Yang, B.; Ma, Y., Solution-Processable Hosts Constructed by Carbazole/PO Substituted Tetraphenylsilanes for Efficient Blue Electrophosphorescent Devices. *Adv. Funct. Mater.* **2014,** 24, 5881-5888.
46. Kim, M.; Lee, J. Y., Engineering the Substitution Position of Diphenylphosphine Oxide at Carbazole for Thermal Stability and High External Quantum Efficiency Above 30% in Blue Phosphorescent Organic Light-Emitting Diodes. *Adv. Funct. Mater.* **2014,** 24, 4164-4169.
47. Gong, S.; Sun, N.; Luo, J.; Zhong, C.; Ma, D.; Qin, J.; Yang, C., Highly Efficient Simple-Structure Blue and All-Phosphor Warm-White Phosphorescent Organic Light-Emitting Diodes Enabled by Wide-Bandgap Tetraarylsilane-Based Functional Materials. *Adv. Funct. Mater.* **2014,** 24, 5710-5718.
48. Fan, C.; Zhu, L.; Liu, T.; Jiang, B.; Ma, D.; Qin, J.; Yang, C., Using an Organic Molecule with Low Triplet Energy as a Host in a Highly Efficient Blue Electrophosphorescent Device. *Angew. Chem. Int. Ed.* **2014,** 53, 2147-2151.
49. Yang, W.; Zhang, Z.; Han, C.; Zhang, Z.; Xu, H.; Yan, P.; Zhao, Y.; Liu, S., Controlling optoelectronic properties of carbazole-phosphine oxide hosts by short-axis substitution for low-voltage-driving PHOLEDs. *Chem. Commun.* **2013,** 49, 2822-2824.
50. Wada, A.; Yasuda, T.; Zhang, Q.; Yang, Y. S.; Takasu, I.; Enomoto, S.; Adachi, C., A host material consisting of a phosphinic amide directly linked donor-acceptor structure for efficient blue phosphorescent organic light-emitting diodes. *J. Mater. Chem. C* **2013,** 1, 2404-2407.
51. Tao, Y.; Xiao, J.; Zheng, C.; Zhang, Z.; Yan, M.; Chen, R.; Zhou, X.; Li, H.; An, Z.; Wang, Z.; Xu, H.; Huang, W., Dynamically Adaptive Characteristics of Resonance Variation for Selectively Enhancing Electrical Performance of Organic Semiconductors. *Angew. Chem. Int. Ed.* **2013,** 52, 10491-10495.
52. Yu, D.; Zhao, F.; Han, C.; Xu, H.; Li, J.; Zhang, Z.; Deng, Z.; Ma, D.; Yan, P., Ternary Ambipolar Phosphine Oxide Hosts Based on Indirect Linkage for Highly Efficient Blue Electrophosphorescence: Towards High Triplet Energy, Low Driving Voltage and Stable Efficiencies. *Adv. Mater.* **2012,** 24, 509-514.
53. Sasabe, H.; Toyota, N.; Nakanishi, H.; Ishizaka, T.; Pu, Y.-J.; Kido, J., 3,3′-Bicarbazole-Based Host Materials for High-Efficiency Blue Phosphorescent OLEDs with Extremely Low Driving Voltage. *Adv. Mater.* **2012,** 24, 3212-3217.

54. Jeon, S. O.; Lee, J. Y., Phosphine oxide derivatives for organic light emitting diodes. *J. Mater. Chem.* **2012,** 22, 4233-4243.
55. Han, C.; Zhang, Z.; Xu, H.; Yue, S.; Li, J.; Yan, P.; Deng, Z.; Zhao, Y.; Yan, P.; Liu, S., Short-Axis Substitution Approach Selectively Optimizes Electrical Properties of Dibenzothiophene-Based Phosphine Oxide Hosts. *J. Am. Chem. Soc.* **2012,** 134, 19179-19188.
56. Han, C.; Zhang, Z.; Xu, H.; Li, J.; Xie, G.; Chen, R.; Zhao, Y.; Huang, W., Controllably Tuning Excited-State Energy in Ternary Hosts for Ultralow-Voltage-Driven Blue Electrophosphorescence. *Angew. Chem. Int. Ed.* **2012,** 51, 10104-10108.
57. Zhao, J.; Xie, G.-H.; Yin, C.-R.; Xie, L.-H.; Han, C.-M.; Chen, R.-F.; Xu, H.; Yi, M.-D.; Deng, Z.-P.; Chen, S.-F.; Zhao, Y.; Liu, S.-Y.; Huang, W., Harmonizing Triplet Level and Ambipolar Characteristics of Wide-Gap Phosphine Oxide Hosts toward Highly Efficient and Low Driving Voltage Blue and Green PHOLEDs: An Effective Strategy Based on Spiro-Systems. *Chem. Mater.* **2011,** 23, 5331-5339.
58. Swensen, J. S.; Polikarpov, E.; Von Ruden, A.; Wang, L.; Sapochak, L. S.; Padmaperuma, A. B., Improved Efficiency in Blue Phosphorescent Organic Light-Emitting Devices Using Host Materials of Lower Triplet Energy than the Phosphorescent Blue Emitter. *Adv. Funct. Mater.* **2011,** 21, 3250-3258.
59. Jeon, S. O.; Jang, S. E.; Son, H. S.; Lee, J. Y., External Quantum Efficiency Above 20% in Deep Blue Phosphorescent Organic Light-Emitting Diodes *Adv. Mater.* **2011,** 23, 1436-1441.
60. Jeon, S. O.; Yook, K. S.; Joo, C. W.; Lee, J. Y., High-Efficiency Deep-Blue-Phosphorescent Organic Light-Emitting Diodes Using a Phosphine Oxide and a Phosphine Sulfide High-Triplet-Energy Host Material with Bipolar Charge-Transport Properties. *Adv. Mater.* **2010,** 22, 1872-1876.
61. Chou, H.-H.; Cheng, C.-H., A Highly Efficient Universal Bipolar Host for Blue,Green, and Red Phosphorescent OLEDs. *Adv. Mater* **2010,** 22, 2468-2471.
62. Jeon, S. O.; Yook, K. S.; Joo, C. W.; Lee, J. Y., Phenylcarbazole-Based Phosphine Oxide Host Materials For High Efficiency In Deep Blue Phosphorescent Organic Light-Emitting Diodes. *Adv. Funct. Mater.* **2009,** 19, 3644-3649.
63. Hsu, F.-M.; Chien, C.-H.; Shu, C.-F.; Lai, C.-H.; Hsieh, C.-C.; Wang, K.-W.; Chou, P.-T., A Bipolar Host Material Containing Triphenylamine and Diphenylphosphoryl-Substituted Fluorene Units for Highly Efficient Blue Electrophosphorescence. *Adv. Funct. Mater.* **2009,** 19, 2834-2843.
64. Li, J.; Ding, D.; Wei, Y.; Zhang, J.; Xu, H., A "Si-Locked" Phosphine Oxide Host with Suppressed Structural Relaxation for Highly Efficient Deep-Blue TADF Diodes. *Adv. Opt. Mater.* **2016**, 4, 522-528.
65. Sun, M.; Zhu, L.; Kan, W.; Wei, Y.; Ma, D.; Fan, X.; Huang, W.; Xu, H., Ternary donor-acceptor phosphine oxide hosts with peculiar high energy gap for efficient blue electroluminescence. *J. Mater. Chem. C* **2015,** 3, 9469-9478.
66. Duan, C.; Fan, C.; Wei, Y.; Han, F.; Huang, W.; Xu, H., Optimizing the Intralayer and Interlayer Compatibility for High-Efficiency Blue Thermally Activated Delayed Fluorescence Diodes. *Sci. Rep.* **2016,** 6, 19904.
67. Han, C.; Zhao, Y.; Xu, H.; Chen, J.; Deng, Z.; Ma, D.; Li, Q.; Yan, P., A Simple Phosphine–Oxide Host with a Multi-insulating Structure: High Triplet Energy Level for Efficient Blue Electrophosphorescence. *Chem. Eur. J.* **2011,** 17, 5800-5803.

68. An, Z.; Zheng, C.; Tao, Y.; Chen, R.; Shi, H.; Chen, T.; Wang, Z.; Li, H.; Deng, R.; Liu, X.; Huang, W., Stabilizing triplet excited states for ultralong organic phosphorescence. *Nat Mater* **2015,** 14, 685-690.
69. Peach, M. J. G.; Tozer, D. J., Overcoming Low Orbital Overlap and Triplet Instability Problems in TDDFT. *J. Phys. Chem. A* **2012,** 116, 9783-9789.
70. Sun, H.; Zhong, C.; Brédas, J.-L., Reliable Prediction with Tuned Range-Separated Functionals of the Singlet–Triplet Gap in Organic Emitters for Thermally Activated Delayed Fluorescence. *J. Chem. Theory Comput.* **2015,** 11, 3851-3858.
71. Nakagawa, T.; Ku, S.-Y.; Wong, K.-T.; Adachi, C., Electroluminescence based on thermally activated delayed fluorescence generated by a spirobifluorene donor-acceptor structurew. *Chem. Commun.* **2012,** 48, 9580-9582.
72. Zhang, J.; Ding, D.; Wei, Y.; Han, F.; Xu, H.; Huang, W., Multiphosphine-Oxide Hosts for Ultralow-Voltage-Driven True-Blue Thermally Activated Delayed Fluorescence Diodes with External Quantum Efficiency beyond 20%. *Adv. Mater.* **2016,** 28, 479-485.
73. Li, J.; Ding, D.; Tao, Y.; Wei, Y.; Chen, R.; Xie, L.; Huang, W.; Xu, H., A Significantly Twisted Spirocyclic Phosphine Oxide as a Universal Host for High-Efficiency Full-Color Thermally Activated Delayed Fluorescence Diodes. *Adv. Mater.* **2016,** 28, 3122-3130.

SYNOPSIS. **P=O jointed blue thermally activated delayed fluorescence (TADF) emitter** 10,10',10"-(4,4',4"-phosphoryltris(benzene-4,1-diyl))tris(10H-phenoxazine) (**TPXZPO**) is constructed to demonstrate the feasibility and flexibility of weak acceptor-strong donor (WASD) strategy for blue TADF dyes. At the same time of preserving blue emission, the enhanced intramolecular charge transfer (ICT) in multi-dipolar **TPXZPO** facilitates the reverse intersystem crossing (RISC) for efficient TADF emission, rendering the high efficiencies for its blue and white devices.